Coherence and Correlations in Atom Lasers

P. D. Drummond[1], T. Vaughan[1], J. F. Corney[1], G. Leuchs[2], P. Deuar[3]

[1]*ARC Centre of Excellence for Quantum-Atom Optics, The University of Queensland, Brisbane QLD 4072, Australia,*
[2]*Max-Planck Forschungsgruppe, Universitat Erlangen-Nurnberg,*
[3]*Laboratoire de Physique Théorique et Modèles Statistiques,*
Université Paris-Sud, 91405 Orsay cedex, France.

drummond@physics.uq.edu.au

Abstract: We review and characterize the quantum coherence measures that are most useful for quantum gases, including Bose-Einstein condensates (BEC) and ultra-cold fermions, and outline how to calculate these in the typically dynamical environment of an interacting multi-mode quantum gas.

1. Introduction

Understanding the coherence and correlations of ultra-cold quantum gases can be thought of as an extension of Glauber's seminal work [1–3] on the quantum coherence properties of photons. Indeed, the basic measured quantities are the quantum correlation functions of the gas, [4] just as in the photonic systems treated by Glauber.

We start with the fundamental principle that particle detection experiments measure n-th order correlations*:*

$$G^{(n)}(\mathbf{x}_1 \ldots \mathbf{x}_n, \mathbf{x}_{n+1}, \ldots \mathbf{x}_{2n}) = \left\langle \hat{\Psi}^\dagger(\mathbf{x}_1)\hat{\Psi}^\dagger(\mathbf{x}_n)\hat{\Psi}(\mathbf{x}_{n+1})\ldots\hat{\Psi}(\mathbf{x}_{2n})\right\rangle \tag{1}$$

If $\mathbf{x}_n = \vec{x}_n, t_n$, then these normally-ordered correlations correspond to an absorptive measurement of n particles, at n distinct space-time events. Nonabsorptive measurements are simply density correlations [5], but we will focus on the normally ordered correlations for definiteness. They then can be used to define normalized correlation measures:

$$g^{(n)}(\mathbf{x}_1 \ldots \mathbf{x}_n, \mathbf{x}_{n+1}, \ldots \mathbf{x}_{2n}) = \frac{G^{(n)}(\mathbf{x}_1 \ldots \mathbf{x}_n, \mathbf{x}_{n+1}, \ldots \mathbf{x}_{2n})}{\sqrt{\prod_i G^{(1)}(\mathbf{x}_i, \mathbf{x}_i)}} \tag{2}$$

In particular, we wish to ask: what correlations *characterize* an N-particle ultra-cold gas? Given that, in principle, all correlation functions are measurable, we must focus on those that convey useful information. We will investigate center-of-mass measurements, condensation measurements, and pair-correlation properties.

Thus, the main questions of interest here are:

- Center-of-mass position and momentum
  - What is the 'standard quantum limit' for position measurement?
  - We find that fermions with a given density distribution have a lower variance than bosons.
- Measures of condensation into a single mode, or orbital, as in a BEC
  - How can one measure Bose condensation into an unknown single-particle state?
  - We show that one should use higher-order correlations to characterize a condensate in general, under conditions that the condensed mode is unknown and may have statistical fluctuations!
- Dynamical correlations in quantum nonlinear **atom** optics
  - How can one calculate statistical correlations that vary in time, in quantum dynamical experiments?
  - We show that non-classical phase-space representations provide powerful methods for these calculations.

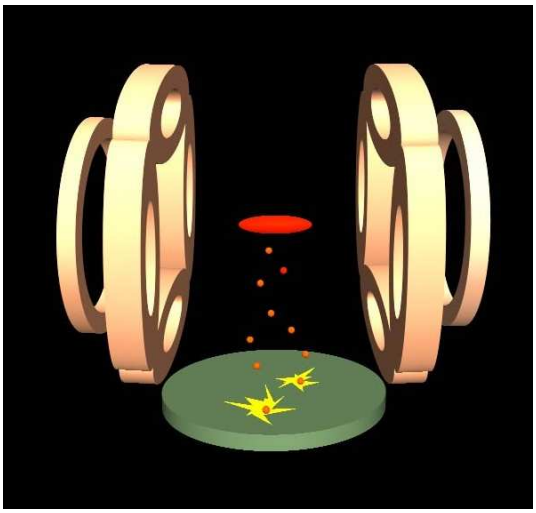

Figure 1. Schematic diagram of metastable Helium experiments.

2. Ultra-cold Atom Experiments

The simplicity of ultracold quantum gases is a vital factor in modern developments in this field. Theoretical descriptions are able to use simple models [6,7], combining coherence and many-body theory. The underlying interactions are well characterized by a few parameters, interactions can be tuned, and new (possibly macroscopic) tests of quantum mechanics are possible [8].

Recent developments include the well known experiments that have led to atom lasers, atomic diffraction, and interferometers. However, a quiet revolution in measurement techniques has also taken place, leading to the direct detection of atom correlations. This allows us to ask what quantifies the location, coherence and correlations of an ultra-cold gas at the quantum noise level, with an assurance that the corresponding measurements are not impossible.

Thus, the driving force behind theoretical efforts to characterize the coherence and correlation properties of ultra-cold quantum gases is the rapid growth in experimental techniques, for both generating ultra-cold gases and carrying out the requisite correlation measurements.

The first technique for measuring atomic correlations in cold gases was the pioneering Hanbury-Brown-Twiss two-atom correlation experiment carried out by Yasuda and Shimizu [9] on an ultra-cold metastable $^{20}Ne^*$ atomic beam. More recently, the development of multi-channel plate He^* atom counting techniques [10] now allows the direct measurement of space and time-resolved arrivals of either fermonic or bosonic metastable Helium atoms on a detector plate, as shown in Fig (1). While these methods still have some limitations with regard to efficiency and time-resolution, they are in principle able to count almost every atom in a metastable ultra-cold gas.

The first technique for measuring atomic correlations *inside* a non-metastable Bose condensate was the use of ultra-cold collisions as a loss-mechanism, proportional to the local correlation function. This can be used either directly, or in combination with photo-association methods. It typically provides spatially integrated information, averaged over a trap volume. As an example, this method was used to measure $g^{(3)}$using three-body collisions [11], thus providing the first evidence for the correlations predicted [12] in the Tonk-Girardeau regime in a one-dimensional Bose gas.

Another technique of great interest is the use of optical probes. Such measurements are sensitive to the local density fluctuations, and were historically used first to study liquids and particles in suspension via light scattering. Modern techniques typically focus on forward scattering, and have been used to measure nonlocal density correlations between fermion pairs [13,14] produced in molecular 'downconversion' experiments, analogous to parametric downconversion in optics, and also between bosonic atoms [15–18]. Other, more exotic correlation measurement techniques are also under development [19,20].

While undoubtedly more complex than a simple BEC-formation experiment, all of these different atom correlation experiments are still table-top compatible, as shown in Fig (2), which illustrates a compact metastable Helium correlation experiment at the Australian National University.

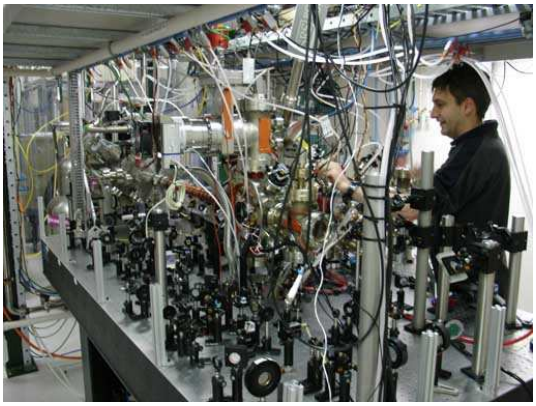

Figure 2. Tabletop setup for metastable Helium experiment.

3. Center of mass measures

In ultra-cold atom experiments, the BEC or degenerate Fermi gas is not homogeneous, because of the trap, and is therefore spatially localized. This introduces the first idea we wish to explore: what is the standard quantum limit [21] for a center-of-mass (COM) position and momentum measurement? The relevant Hermitian operators, for the case of a number state with eigenvalue $N > 0$, are:

$$\begin{aligned} \hat{\mathbf{x}}^{(N)} &= \frac{\int \mathbf{x}\hat{n}(\mathbf{x})d^D\mathbf{x}}{N}, \\ \hat{\mathbf{P}} &= \hbar \int \mathbf{k}\hat{n}(\mathbf{k})d^D\mathbf{k}, \end{aligned} \tag{3}$$

where $\hat{n}(\mathbf{x}) = \hat{\Psi}^\dagger(\mathbf{x})\hat{\Psi}(\mathbf{x})$. Here the spatial dimension D is included to allow treatment of reduced dimensional environments. These collective operators obey the usual commutation relations:

$$[\hat{x}_j^{(N)}, \hat{P}_k] = i\hbar\delta_{jk} \tag{4}$$

and Heisenberg Uncertainty Principle:

$$\Delta x_i^{(N)} \Delta P_i \geq \frac{\hbar}{2} \tag{5}$$

When there is an uncertainty in the total particle number, a useful approximation (for large numbers of particles) is to replace the eigenvalue by the mean operator expectation value:

$$\hat{X} = \frac{1}{\langle \hat{N} \rangle} \int \mathbf{x}\hat{n}(\mathbf{x})d^D\mathbf{x} \tag{6}$$

3.1. Standard Quantum Noise Levels

We wish to find the characteristic or 'standard' quantum noise level (SQNL) for the COM position and momentum variance, in an idealized low-noise state. This is analogous to the vacuum noise level of a quadrature measurement. That is, while it is not the lowest noise level possible - which is zero - it is a reasonable goal for an experiment in which technical and thermal noise are eliminated as far as possible. We consider a SQNL defined relative to given density distribution $\langle \hat{n}(\mathbf{x}) \rangle$, as the COM variance of the ground-state system configuration in a non-interacting gas with the same density.

Given this definition as the characteristic noise level, we wish to compare the cases of Fermi and Bose gases. Now the SQNL as defined here does not require the gas to be trapped - the gas could be in free space. However, the reference system we choose for comparison purposes is a trapped, non-interacting gas for simplicity. We note that it is possible to have the system in a minimum uncertainty state, which satisfies Eq (5) replaced by an equality. Quantum states that are analogous to squeezed states are also possible, in which there is a trade-off between reduction in one variance, and increase in the other.

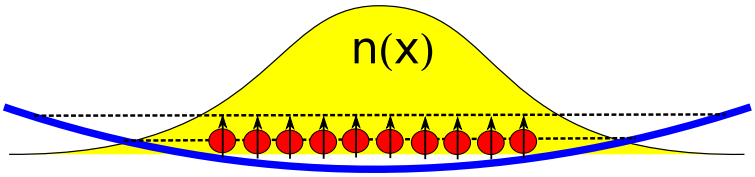

Figure 3. Identical bosons in their ground state.

Experimentally, the existence of excess noise from the initial atomic source, a moving trap potential, residual thermal noise or even from the quantum noise of the cooling process itself, can result in excess momentum injected into the atomic cloud. This will cause micro-motion in the trap, and hence a COM variance for both the position and momentum which is above the standard limit. Repeated measurements on an ensemble will result in different values of position and momentum, for each measurement, with the possible outcome that both types of variance are well above the SQNL.

However, the simple question we will investigate here is the value of the variance in the case of a non-interacting ground-state configuration.

3.2. SQNL - Identical Bosons

We introduce the notation of

$$\hat{a}_j = \int \hat{\Psi}(\mathbf{x})\, u_j^*(\mathbf{x})\, d^D\mathbf{x}, \tag{7}$$

where $u_j(\mathbf{x})$is lowest single-particle energy eigenstate of the nominal potential used to obtain the required density distribution.

The reference ground state, corresponding to N identical bosons in the single-particle ground state (shown schematically in Fig 3) is then:

$$|\Psi^{(N)}\rangle = \frac{1}{\sqrt{n!}}\left[\hat{a}_0^\dagger\right]^N |0\rangle, \tag{8}$$

for which the SQNL for mean position and momentum in any dimension is:

$$\begin{aligned} \sigma_{Sx}^2 &= \langle \Delta\hat{x}_i^2 \rangle = \sigma_x^2/N \\ \sigma_{Sp}^2 &= \langle \Delta\hat{P}_i^2 \rangle = N\sigma_p^2 \end{aligned} \tag{9}$$

Here σ_p is the standard deviation of the density distribution in momentum space, equal to $\hbar/(2\sigma_x)$ if the distribution is Gaussian (and thus in a minimum uncertainty state).

3.3. SQNL - Identical Fermions

We can express the zero-temperature state of a collection of N identical fermions using a similar notation:

$$|\Psi^{(N)}\rangle = \left[\prod_{j=1}^{N} \hat{a}_j^\dagger\right] |0\rangle \tag{10}$$

where j labels the N lowest energy eigenstates of some trapping potential, as shown in figure 4. For simplicity here, we assume the potential $V(\mathbf{x}) = \hbar\omega^2 |\mathbf{x}|^2/2$ is harmonic, with a trap-frequency ω.

The dimensionality of the calculation in this case influences the result through the mode structure of the ground state of N identical fermions. For a Fermi gas confined to D spatial dimensions, the SQNL in the mean position and total momentum is

$$\begin{aligned} \sigma_{Sx}^2 &= \langle \Delta\hat{x}_i^2 \rangle = \sigma_x^2/N^{1+1/D} \\ \sigma_{Sp}^2 &= \langle \Delta\hat{P}_i^2 \rangle = N^{1-1/D}\sigma_p^2\,. \end{aligned} \tag{11}$$

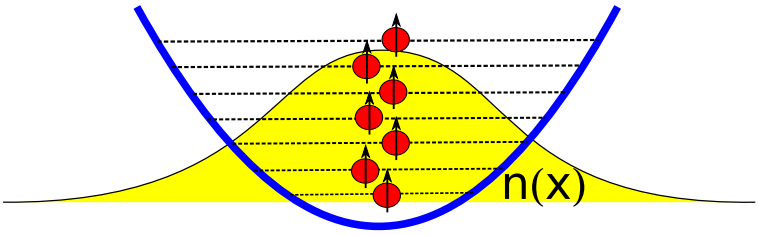

Figure 4. Identical harmonically trapped fermions in their ground state.

We thus find the interesting result that the SQNL in measurements of the mean position is a factor of $\sqrt[D]{N}$ smaller for harmonically trapped fermions in comparison with the same number of identical bosons - ie., N times smaller in one dimension - provided the density variance itself is comparable. We attribute this difference to the Pauli exclusion principle and the associated Fermi pressure which expands the density distribution (for the same trap frequency), but with correlated density fluctuations so that the mean COM variance is unchanged. In the Fermi case, the expanded size means that $\sigma_p \sim N^{1/D}\hbar/(2\sigma_x)$, so that the density distribution variances are no longer at the minimum uncertainty level. However, the minimum uncertainty limit for COM position and momentum is (approximately) achieved for a harmonic trap in any number of dimensions.

Surprisingly, it is the characteristic length of the trap ground-state (divided by $\sqrt{N}$) that sets the absolute COM position variance scale for either type of quantum statistic.

4. Condensation measures

The archetypal criterion for Bose-Einstein condensation in a gas of interacting identical bosons is the one devoloped in 1956 by Penrose and Onsager [22]. Their criterion hinges on the fact that eigenvalues of the single particle reduced density matrix $\rho^{(1)}(\mathbf{x},\mathbf{x}') = \langle\hat{\psi}^\dagger(\mathbf{x}')\hat{\psi}(\mathbf{x})\rangle$ are the mean occupancies of the corresponding eigenstates. Penrose and Onsager therefore suggested that the existance of BEC is synonymous with at least one of these eigenvalues growing extensively with the size of the system. This is equivalent to requiring perfect first order (phase) coherence, a fact which is reflected in Glauber's extension of his theory of optical coherence [1–3] to the ultra-cold gas arena [4].

The question we now ask is this: is first order coherence the defining feature of a BEC? Recent literature has begun to acknowlege that the answer may in fact be no. For example, Wilkin et al. [23] have found the zero-temperature ground state of an harmonically trapped attractively interacting rotating Bose gas is a fragmented condensate according to the first order criterion. Pethick and Pitaevskii [24] have leveled criticism at this diagnosis, suggesting that the Penrose-Onsager criterion gives sensible results only when interpreted in the centre-of-mass frame of the system. This same result has also been considered in depth by Gajda [25] who suggests that Wilkin et al.'s unintuitive result might be avoided if the reduced density operator in the Penrose-Onsager criterion were replaced with 'conditional' reduced density operators – again effectively tracing out any mean position uncertainty present in the system.

Additionally, the first-principles evaporative cooling simulations discussed later in Sec. 5 provide further evidence of the short-comings of using first-order coherence as the basis for a criterion. They indicate that at least one method of BEC preparation implicitly results in significant mean position uncertainty which washes out the uniform phase coherence.

4.1. Probabilistic mixtures of condensed modes

Examples of states which are handled incorrectly by the Penrose-Onsager criterion can be easily constructed. For instance, consider the following mixed state:

$$\hat{\rho}_M = \sum_i p_i |(u_i)^N\rangle\langle(u_i)^N| \tag{12}$$

where each $|(n_i)^N\rangle = (\hat{a}_i^{\dagger N}/\sqrt{N!})|0\rangle$ describes a condensed N-particle system with the order parameter $u_i(\mathbf{r})$. This is therefore a mixture of condensates in different modes: in every case there is a BEC present.

Such mixtures occur when the center-of-mass motion is excited in a trapped BEC. This motion is undamped, and observed in almost all experiments. It may, under some circumstances, result in a relatively low average occupation of

any single mode. This of course leads to the decay of first-order coherence and thus the condensate fraction as defined by Penrose and Onsager.

We posit, however, that statistical uncertainty as to the exact mode of condensation should not influence the classification of that system as condensed, given the particles deterministically occupy a single mode.

4.2. Higher-order condensation measures

One obvious solution to this problem is to consider measures based on correlations of order greater than unity. For a set of orthogonal modes $u(\mathbf{r})$ we define the m-th order phase-space filling factor

$$F_u^{(m)} = \frac{\sum_u \langle : \hat{n}_u^m : \rangle}{\langle : \hat{N}^m : \rangle}. \tag{13}$$

This is a well-defined, obversable correlation function for the Bose gas that describes the (inverse) spread across the modes $u(\mathbf{r})$ in individual members of a statistical ensemble. It has the property that it is sensitive to off-diagonal number correlations such as $\langle : \hat{n_u} \hat{n}_{u'} \hat{n}_{n''} \ldots : \rangle$ in such a way that the filling factor approaches unity for systems in mixed states composed only of macroscopically occupied modes in this particular basis.

The filling factor is therefore a signature of condensation even when the BEC is oscillating or moving randomly, as it usually is in an experiment, provided the possible condensate modes belong (or are 'close' to) the set of orthogonal modes present in the numerator of $F^{(m)}$. .For example, consider the second-order phase-space filling factor in momentum space:

$$F_{\mathbf{k}}^{(2)} = \frac{\sum_{\mathbf{k}} \langle : \hat{n}_{\mathbf{k}}^2 : \rangle}{\langle : \hat{N}^2 : \rangle} \tag{14}$$

which attains its maximum of one for a state with all of the particles in a single momentum mode, or for a mixture of such states with possibly different values of momentum. This is calculable for models of evaporative cooling and gives a high occupation even for unknown modes.

In terms of spatial correlations, this particular measure can be written as

$$\begin{aligned} F^{(2)} &= \frac{1}{V \langle : \hat{N}^2 : \rangle} \int d\mathbf{x_1} d\mathbf{x_2} d\mathbf{r} \langle \hat{\Psi}^\dagger(\mathbf{x_1} - \mathbf{r}) \hat{\Psi}^\dagger(\mathbf{x_2} + \mathbf{r}) \hat{\Psi}(\mathbf{x_2}) \hat{\Psi}(\mathbf{x_1}) \rangle \\ &= \frac{1}{V \langle : \hat{N}^2 : \rangle} \int d\mathbf{x_1} d\mathbf{x_2} d\mathbf{r} G^{(2)}(\mathbf{x}_1 - \mathbf{r}, \mathbf{x}_2 + \mathbf{r}, \mathbf{x}_2, \mathbf{x}_1), \end{aligned} \tag{15}$$

which is just the spatial average of a second-order nonlocal correlation function. Thus the phase-space filling factor, when defined in terms of the momentum modes, is a measure of the overall spatial coherence of the state. But unlike first-order measures of coherence, it is robust in the presence of mixtures.

5. Simulations of quantum dynamics

While defining relevant correlation functions is both instructive and relatively simple, the same cannot be said for their calculation. We are faced with the problem of how to calculate an interacting many-body quantum state. Furthermore, for ultracold atoms, since there is no coupling to a finite-temperature reservoir, and external potentials and fields are readily adjustable, most experiments are typically non-equilibrium in nature.

The underlying difficulty is that quantum many-body problems are exponentially complex. If we consider n atoms distributed among m modes, and take $n \simeq m \simeq 500,000$, then the corresponding number of distinct quantum states is:

$$N_S \approx 2^{2n} \approx 2^{1,000,000} \tag{16}$$

This means that there are more quantum states than atoms in the universe, so we certainly can't numerically diagonalize the Hamiltonian. Even if we could find the eigenstates, there are so many that this is not of itself particularly useful. Calculating N_S expansion coefficients for an arbitrary initial state is necessary, in order to **use** the eigenstates in a dynamical calculation. This is not a practical endeavour.

As an illustration, Fig (5) gives a diagram of the collision physics that leads to evaporative cooling. However, a typical experiment has not just two, but rather millions of initial atoms (or more). To discover the final quantum density matrix requires one to integrate forward in time a many-body master equation that includes both quantum collisions and trap losses. This can be carried out using a Boltzmann or quantum kinetic equation approximation [26],

but this is usually at some cost in accuracy. While all stochastic approaches sacrifice information, what matters is that no systematic errors are introduced.

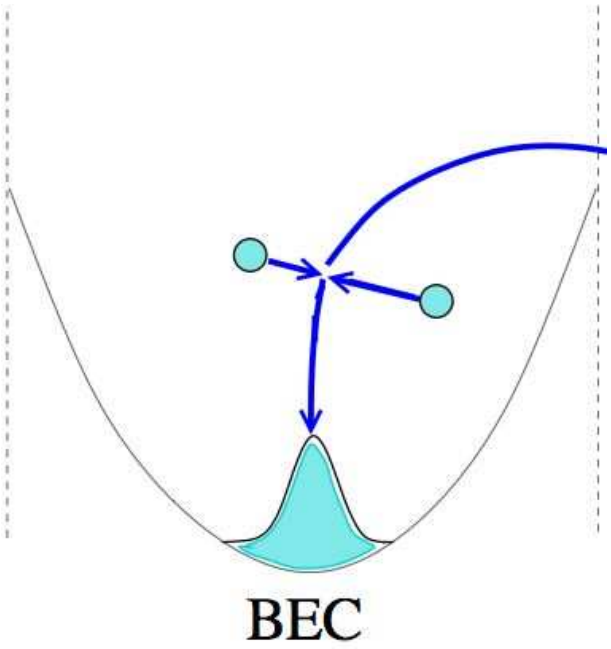

Figure 5. Schematic diagram of evaporative cooling collision

5.1. Quantum phase-space methods

There are a number of phase-space representations of quantum mechanics. However, if a classical phase-space is used, as in the Wigner [27] and Glauber-Sudarshan [28] representations, with $2M$ degrees of freedom (x_i, p_i) for M classical coordinates x_i, one finds that there is in general no exact stochastic process in (x_i, p_i) that corresponds to the quantum dynamics. One way to understand this, is that this would be equivalent to a local hidden variable theory, which is in general ruled out by Bell's theorem. Despite this, these techniques are useful approximations with many applications [29–32]. An alternative method is to use a nonclassical phase-space, that allows for quantum entanglement and superpositions [33, 34].

As an example, the Positive-P representation [33] uses a non-classical phase-space. It is able to represent all quantum density matrices, and has a positive definite propagator. The method expands the density matrix over coherent states $|\vec{\alpha}\rangle$ with $4M$ real or $2M$ complex coordinates:

$$\hat{\rho} = \int P(\vec{\alpha}, \vec{\beta}) \, \frac{|\vec{\beta}\rangle\langle\vec{\alpha}|}{\langle\vec{\alpha}|\vec{\beta}\rangle} \, d^{2M}\vec{\alpha} \, d^{2M}\vec{\beta} \tag{17}$$

The resulting distributions are positive and obey a diffusion equation when the system is described by a Hamiltonian that involves single– and two–particle processes, which can therefore be numerically simulated on a conventional digital computer [35]. A number of useful applications of these methods to correlation function calculations have been made [36–38]. The trade-off is that, when there is insufficient damping, the sampling error increases with time, although the useful time period is easily estimated [39]. This can be controlled, to some extent, with more advanced methods like the stochastic-gauge P-representation [40–42].

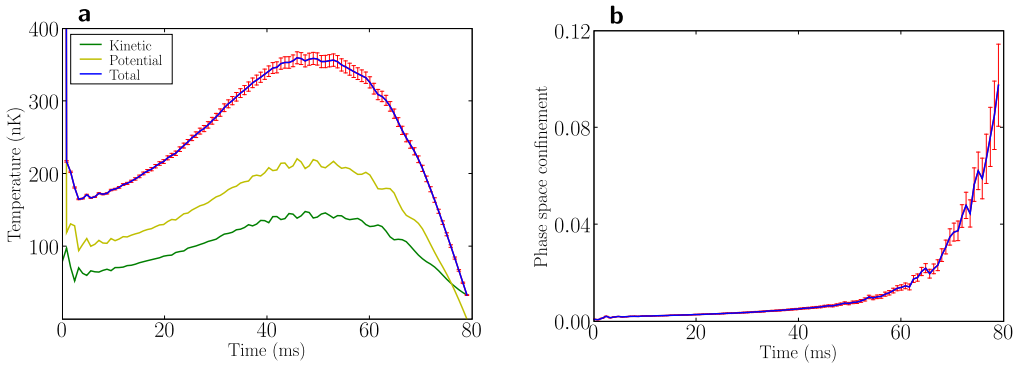

Figure 6. Evaporative cooling simulation results: (a) effective center-of-mass temperature and (b) second-order phase-space filling factor ($F_{\mathbf{k}}^{(2)}$) measure of condensation.

5.2. Evaporative cooling

The breakthrough in experimental techniques which led to the observation of BEC was the use of evaporative cooling to produce temperatures even lower than those obtained with laser cooling. However, as this is a non-equilibrium process - with no conventional thermal reservoir - it leads to an intriguing fundamental question: *What is the true state of an atom BEC?*

We have tried to answer this question with a first-principles quantum simulation of the many-body quantum dynamics leading to BEC formation [43]. The process is simple in principle. As shown in Fig. 5, colliding warm atoms can produce a 'hot' and 'cold' pair: the more energetic atom escapes, while the slow-moving partner joins the condensate. This process is accelerated by Bose stimulation, once there are sufficiently many particles in a low-energy single-particle state.

The system is described by the following Hamiltonian:

$$\hat{H} = \int \left[\frac{\hbar^2}{2m} \nabla\hat{\Psi}^\dagger \nabla\hat{\Psi} + \frac{g}{2}\hat{\Psi}^{\dagger 2}\hat{\Psi}^2 + V(\mathbf{r},t)\hat{\Psi}^\dagger\hat{\Psi} + \hat{\Gamma}(\mathbf{r})\hat{\Psi}^\dagger + \hat{\Gamma}^\dagger(\mathbf{r})\hat{\Psi} \right] d^3\mathbf{r}. \tag{18}$$

Here g represents the inter-atomic s-wave scattering interaction in a point-contact approximation (with a momentum cut-off), m is the mass, $V(\mathbf{r})$ is the trap potential, and $\hat{\Gamma}(\mathbf{r})$ is a reservoir of untrapped modes which describe the spatially dependent out-coupling from the trap. After transforming to the positive-P representation, rescaling to a dimensionless form, sampling the distribution and obtaining the stochastic equations for the samples, one obtains the following equations for the complex fields $\alpha(\mathbf{z},\tau), \beta(\mathbf{z},\tau)$:

$$\begin{aligned} \frac{d\alpha}{d\tau} &= -i\left[\alpha\beta^* + v(\mathbf{z},\tau) - i\gamma(\mathbf{z}) - \nabla^2 + \sqrt{i}\zeta_1(\mathbf{z},\tau)\right]\alpha \\ \frac{d\beta}{d\tau} &= -i\left[\alpha^*\beta + v(\mathbf{z},\tau) - i\gamma(\mathbf{z}) - \nabla^2 + \sqrt{i}\zeta_2(\mathbf{z},\tau)\right]\beta, \end{aligned} \tag{19}$$

where, $\zeta_{(j)}(\mathbf{z},\tau)$ are real independent white noise fields with the variances

$$\langle \zeta_{(i)}(\mathbf{z},\tau)\zeta_{(j)}(\mathbf{z}',\tau')\rangle = \delta_{ij}\delta(\tau-\tau')\delta^{(3)}(\mathbf{z}-\mathbf{z}')\,. \tag{20}$$

Thes equations are an exact mapping from quantum dynamics. They have the structure of the usual Gross-Pitaevskii mean-field equations, together with a stochastic delta-correlated field that contains the quantum noise caused by collisions. These noise terms give rise, for example, to the spontaneous effects that are absent in a mean-field description. There are two coupled phase-space fields driven by independent noises, so that eventually the equations depart from the usual classical GP behaviour. The equations include the scaled trap potential $v(\mathbf{z},\tau)$, and loss rate $\gamma(\mathbf{z})$.

The results of the evaporative cooling simulations are illustrated as Fig. 6. Firstly, Fig. 6 (a) shows the time-dependence of the center-of-mass temperature, showing the presence of a stimulated increase in center-of-mass temperature, during the condensate formation process. Secondly, Fig. 6 (b) illustrates the corresponding change in the second-order phase-space filling factor $F_{\mathbf{k}}^{(2)}$ (defined in Eq. (14) above) during the condensate formation process, showing that this higher-order measure of coherence can indeed provide a signature of condensate formation.

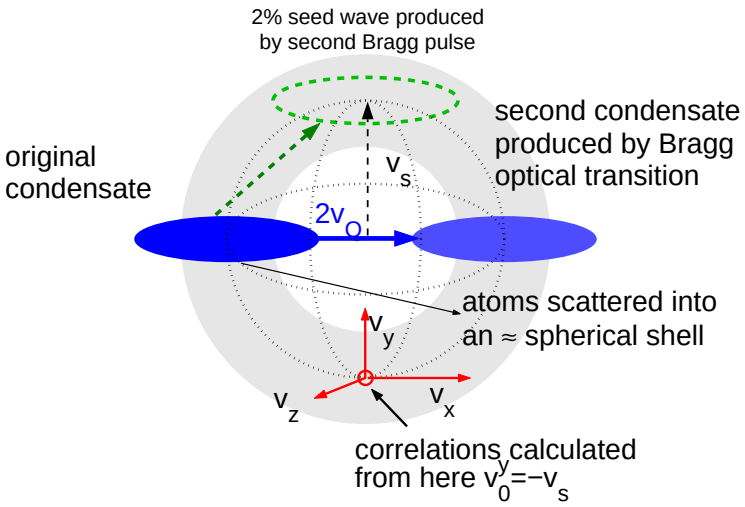

Figure 7. Schematic of the BEC collision

5.3. BEC collisions with 150,000 atoms

The collision of pure ^{23}Na BECs, was reported in an experiment at MIT [44], and a similar setup is now being investigated in detail with metastable He*. This provides an analog to nonlinear optics, in which a type of four-wave mixing occurs, generating correlated pairs of atoms. First-principles quantum dynamical simulations can provide a way to benchmark and test competing approximate theories, while providing a route forward to future experimental tests of correlations. In these simulations [45, 46], schematically represented in Fig. 7, a 1.5×10^6 atom condensate is prepared in a cigar-shaped magnetic trap with frequencies of $20, 80, 80\,Hz$ in the X, Y, Z directions respectively. A brief Bragg laser pulse coherently imparts an X velocity of $2v_Q \approx 20$ mm/s to half of the atoms, which is much greater than the maximum sound velocity of 3.1 mm/s. Simulations of both spontaneous [45] and stimulated [46] scattering were carried out. For stimulated scattering, another much weaker pulse generates a small 2% "seed" wavepacket with a Y velocity of $v_s = 9.37$ mm/s relative to the center of mass (this value is chosen to give strong bosonic stimulation into the “fourth” condensate).

At this point the trap is turned off so that the wavepackets collide freely. In a center-of-mass frame, atoms are scattered preferentially into a spherical shell in momentum space with anticorrelated directions and mean velocities $v_s \approx v_Q$. Seed pulses induce a four-wave mixing process which generates a stimulated coherent wavepacket at Y velocity -v_s, as well as growing the strength of both of the wavepackets at $\pm v_s$ by Bose enhanced scattering.

The dynamics of the distribution of atom velocities and correlations between the scattered atoms have been calculated and are shown in Figures 8. and 9. Such correlations have recently become experimentally measurable [10, 15, 16]. Correlation behaviours qualitatively similar to these have been seen experimentally. The simulation is carried out using the positive-P representation in the X-center-of-mass frame from the moment the lasers and trap are turned off ($t = 0$). The initial wavefunction is modeled as the coherent-state mean-field Gross-Pitaevskii (GP) solution of the trapped $t < 0$ condensate, but modulated with a factor $\left[\sqrt{0.49}e^{imv_Qx/\hbar} + \sqrt{0.49}e^{-imv_Qx/\hbar} + \sqrt{0.02}e^{-imv_sy/\hbar}\right]$ for the case of a 2% seed pulse, or $\sqrt{2}\cos(mv_Qx/\hbar)$ when no seed pulse is present. The field Hamiltonian is discretized with lattice sizes of up to $432\times105\times50$, generating a Hubbard-type Hamiltonian like Eq (18), but with external potential V and reservoirs $\hat{\Gamma}$ omitted.

As mentioned above, limitations arise because the size of the sampling uncertainty grows with time, and eventually, soon after the end of the time scale in Fig. 8, reaches a size where it is no longer practical to obtain useful precision. This time can be estimated using the formulae found in [39], although it may be extended with more sophisticated techniques.

A number of approximate calculations exist for this experiment [30, 31, 47–49], making it useful to have a definitive first-principles approach. Comparisons were made (Fig. 9) with previous approximate simulations that used a scattering cross-section approximation (the SVEA method [47]), and those [30, 31] using a classical phase-space technique - the truncated Wigner method [29]. This approximate method was less accurate (as is to be expected from its limita-

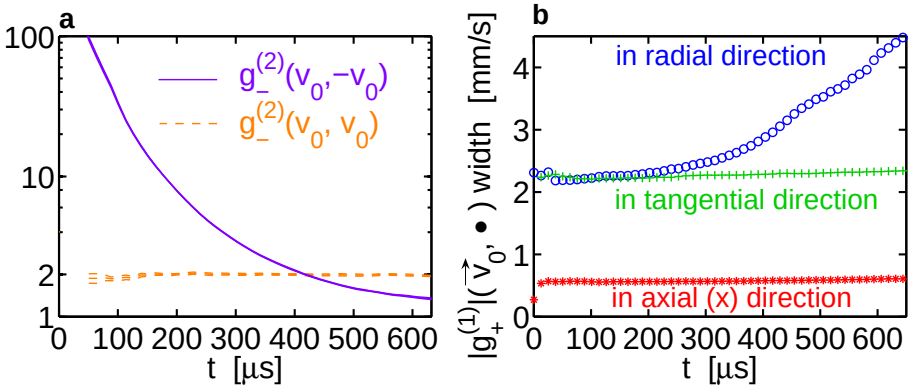

Figure 8. *Correlations between scattered atoms: time evolution (no seed pulse)*. Plate **a** shows the extremely strong number correlations $g^{(2)}(\mathrm{v}_0,-\mathrm{v}_0)$ between atoms with opposite velocity (solid line) in the scattered shell at $|\mathrm{v}_0|=\mathrm{v}_\mathrm{s}$ (away from the coherent wavepackets), and thermal correlations $g^{(2)}(\mathrm{v}_0,\mathrm{v}_0)=2$ between scattered atoms at the same velocity (dashed). Triple lines indicate uncertainty. Plate **b** shows the coherence width in velocity space for scattered atoms at similar velocities centered around v_0. Plotted is the Full-width at half-maximum (FWHM) of $|g^{(1)}(\mathrm{v}_0,\mathrm{v}_0+\mathrm{v})|$.

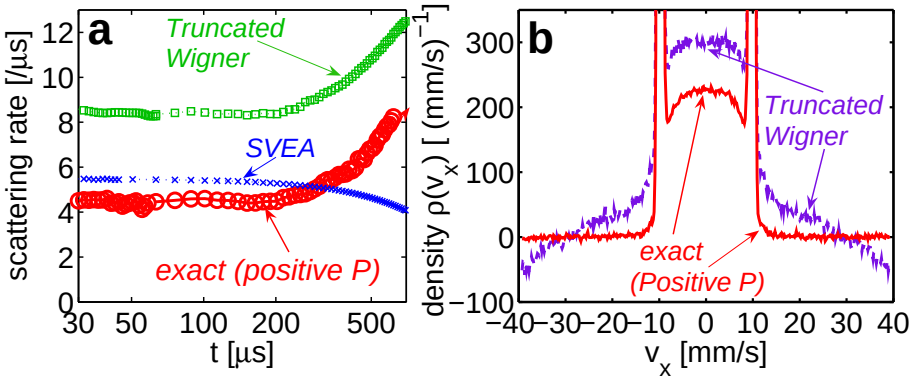

Figure 9. *Scattering rates: time evolution (no seed pulse)*. Plate **a** shows total scattering rates in different approximations compared to the exact positive-P simulations. Plate **b** shows the distribution in velocity space for scattered atoms, demonstrating that the false scattered halo of the truncated Wigner method is caused by an unphysical depletion of the vacuum with negative populations.

tions when the number of particles per mode is small [50]) at large momentum cutoff, due to a diverging truncation error caused by the ultra-violet divergence of the symmetrically-ordered vacuum fluctuations, causing an unphysical depletion of the vacuum modes at high momentum.

The model treated up to $M = 2.268 \times 10^6$ interacting momentum modes. Since each of the $N = 1.5 \times 10^5$ atoms can be in any one of the modes, the Hilbert space contains about $N_s \approx M^N \approx 10^{1,000,000}$ orthogonal quantum states. This demonstrates the ability of nonclassical phase-space methods to simulate quantum mechanical correlations even in the face of exceptionally large many-body Hilbert spaces.

6. SUMMARY

In summary, we have pointed out how pioneering twentieth century developments of coherence and quantum optics are now growing to include ultra-cold atomic coherence and correlations. The field has been greatly enriched by the outstanding efforts of experimentalists to produce atomic gases at ultra-low temperatures, and more recently, to measure their correlations. As the field is a rapidly growing one, we cannot attempt to cover all the new developments, but rather have provided a selection of topics.

A simple idea treated here is to consider the standard quantum limits to center-of mass measurements. We found that for the same density distribution, the ground-state center-of-mass measurement variance is N times lower for a one-dimensional Fermi gas as for a Bose gas of N atoms.

Next, we briefly reviewed how coherence theory can be used to identify Bose condensation. While the traditional Penrose-Onsager measure of first-order coherence is very useful for a restricted class of condensates, it fails to identify condensation within mixtures. We have shown how higher-order coherence theory can be used to define condensation in more general cases.

In order to illustrate how to calculate atomic correlations, we considered the issues raised by the relatively strong inter-atomic interactions, compared to those in quantum optics. In order to include quantum coherence fully, we turn have turned to nonclassical phase-space methods using the positive-P representation. This can handle three-dimensional simulations with up to 10^5 particles, and 10^6 modes, giving conditions close to those found in experiments.

Particular cases presented here include evaporative cooling and condensate formation, which we have found is accompanied by heating of the COM motion. We have also calculated measures of second order quantum coherence in BEC collisions, and shown how the exact results can differ from various approximations.

Acknowledgments

P. Deuar acknowledges financial support by the European Community under the contract MEIF-CT-2006-041390. P. D. D., J.C. and T.V. acknowledge support from the Australian Research Council Centre of Excellence program.

References

1. R. J. Glauber, Phys. Rev. **130**, 2529 (1963).
2. R. J. Glauber, Phys. Rev. **131**, 2766 (1963).
3. U. M. Tittulaer and R. J. Glauber, Phys. Rev. **140**, B676 (1965).
4. M. Naraschewski and R. J. Glauber, Phys. Rev. A **59**, 4595 (1999).
5. E. Altman, E. Demler, and M. D. Lukin, Phys. Rev. A **70**, 013603 (2004).
6. F. Dalfovo *et al.*, Rev. Mod. Phys. **71**, 463 (1999).
7. A. J. Leggett, Rev. Mod. Phys. **73**, 307 (2001).
8. K. V. Kheruntsyan, M. K. Olsen, and P. D. Drummond, Phys. Rev. Lett. **95**, 150405 (2005); E. G. Cavalcanti and M. D. Reid, Phys. Rev. Lett. **97**, 170405 (2006).
9. M. Yasuda and F. Shimizu, Phys. Rev. Lett. **77**, 3090 (1996).
10. M. Schellekens, R. Hoppeler, A. Perrin, J. Viana Gomes, D. Boiron, A. Aspect, C. I. Westbrook, Science **310**, 648 (2005); J. Viana Gomes, A. Perrin, M. Schellekens, D. Boiron, C. I. Westbrook, and M. Belsley, Phys. Rev. A **74**, 053607 (2006); T. Jeltes, J. M. McNamara, W. Hogervorst, W. Vassen, V. Krachmalnicoff, M. Schellekens, A. Perrin, H. Chang, D. Boiron, A. Aspect, Nature **445,** 402 (2007).
11. B. L. Tolra, K. M. O'Hara, J. H. Huckans, W. D. Phillips, S. L. Rolston, and J. V. Porto, Phys. Rev. Lett. **92**, 190401 (2004); Toshiya Kinoshita, Trevor Wenger, and David S. Weiss, Phys. Rev. Lett. **95**, 190406 (2005).
12. K. V. Kheruntsyan, D. M. Gangardt, P. D. Drummond, and G. V. Shlyapnikov, Phys. Rev. Lett. **91**, 040403 (2003).

13. C. A. Regal, J. T. Stewart, and D. S. Jin, Physical Review Letters **94**, 110401 (2005).
14. T. Rom, Th. Best, D. van Oosten, U. Schneider, S. Folling, B. Paredes, I. Bloch, Nature **444**, 733 (2006).
15. M. Greiner *et al.*, Phys. Rev. Lett. **94**, 110401 (2005).
16. S. Fölling, F. Gerbier, A. Widera, O. Mandel, T. Gericke, I. Bloch, Nature **434**, 481 (2005).
17. A. Ottl, S. Ritter, M. Kohl, and T. Esslinger, Phys. Rev. Lett. **95**, 090404 (2005).
18. J. Esteve, J.-B. Trebbia, T. Schumm, A. Aspect, C. I. Westbrook, and I. Bouchoule, Phys. Rev. Lett. **96**, 130403 (2006).
19. Trygve Ristroph, Anne Goodsell, J. A. Golovchenko, and Lene Vestergaard Hau, Phys. Rev. Lett. **94**, 066102 (2005).
20. T. P. Meyrath, F. Schreck, J. L. Hanssen, C.-S. Chuu, and M. G. Raizen, Phys. Rev. A **71**, 041604 (2005).
21. T. Vaughan, P. D. Drummond, G. Leuchs, Phys. Rev. A **75**, 033617 (2007).
22. O. Penrose and L. Onsager, Phys. Rev. **104**, 576 (1956).
23. N. K. Wilkin, J. M. F. Gunn and R. A. Smith, Phys. Rev. Lett. **80**, 2265 (1998).
24. C. J. Pethick and L. P. Pitaevskii, Phys. Rev. A **62**, 033609 (2000).
25. M. Gajda, Phys. Rev. A **73**, 023603 (2006).
26. C. W. Gardiner and P. Zoller, Phys. Rev. A **58**, 536 (1998).
27. E. Wigner, Phys. Rev. **40**, 749 (1932).
28. R. J. Glauber, Phys. Rev. **131**, 2766 (1963); E. C. G. Sudarshan, Phys. Rev. Lett. **10**, 277 (1963).
29. P. D. Drummond, A. D. Hardman, Europhys. Lett. **21**, 279 (1993).
30. A. A. Norrie, R. J. Ballagh, C. W. Gardiner, Phys. Rev. Lett. **94**, 040401 (2005).
31. A. A. Norrie, R. J. Ballagh, C. W. Gardiner, Phys. Rev. A **73**, 043617 (2006).
32. L. Isella, J. Ruostekoski, Phys. Rev. A **72**, 011601(R) (2005).
33. P. D. Drummond, C. W. Gardiner, J. Phys. A: Math. Gen. **13**, 2353 (1980).
34. I. Carusotto, Y. Castin, J. Dalibard, Phys. Rev. A **63**, 023606 (2001).
35. C. W. Gardiner, P. Zoller, *Quantum Noise* (Springer, Berlin, 2004).
36. U. V. Poulsen, K. Molmer, Phys. Rev. A **63**, 023604 (2001); **64**, 013616 (2001).
37. M. R. Dowling *et al.*, Phys. Rev. Lett. **94**, 130401 (2005).
38. C. M. Savage, P. E. Schwenn, and K. V. Kheruntsyan, Phys. Rev. A **74**, 033620 (2006).
39. P. Deuar, P. D. Drummond, J. Phys. A **39**, 1163 (2006).
40. P. Deuar, P. D. Drummond, Phys. Rev. A **66**, 033812 (2002).
41. P. D. Drummond, P. Deuar, J. Opt. B: Quantum Semiclass. Opt. **5**, S281 (2003).
42. P. Deuar, P. D. Drummond, J. Phys. A **39**, 2723 (2006)
43. P. D. Drummond, J. F. Corney, Phys. Rev. A **60**, R2661 (1999).
44. J. M. Vogels, K. Xu, W. Ketterle, Phys. Rev. Lett. **89**, 020401 (2002).
45. P. Deuar and P. D. Drummond, Phys. Rev. Lett. **98**, 120402 (2007).
46. P. D. Drummond, P. Deuar and J. F. Corney, to be published in Opt. and Spectroscopy, arXiv:quant-ph/0608247
47. Y. B. Band *et al.*, Phys. Rev. Lett. **84**, 5462 (2000); T. Köhler, K. Burnett, Phys. Rev. A **65**, 033601 (2002).
48. R. Bach, M. Trippenbach, K. Rzażewski, Phys. Rev. A **65**, 063605 (2002).
49. P. Ziń *et al.*, Phys. Rev. Lett. **94**, 200401 (2005).
50. A. Sinatra, C. Lobo, Y. Castin, J. Phys. B **35**, 3599 (2002).